AIAA Guidance, Navigation, and Control Conference
2 - 5 August 2010, Toronto, Ontario Canada

AIAA 2010-8068

Simulation of Multibody Spacecraft Reconfiguration through Sequential Dynamic Equilibria

Joseph P. Shoer[1] and Mason A. Peck[2]
Cornell University, Ithaca, NY, 14853

This paper describes a novel hybrid-control strategy to reconfigure multibody spacecraft from one shape to another in such a way that passively stable system dynamics enable both low control effort and a high degree of robustness. This approach treats reconfigurable spacecraft systems as multibody kinematic mechanisms with controllable kinematics and takes advantage of ambient force fields in the space environment (gravity gradient, magnetism, etc.) along with passively generated, non-contacting forces on the spacecraft (such as those from permanent magnets) to drive the reconfiguration maneuver to one stable dynamic equilibrium after another, in sequence. The use of kinematic constraints and passive dynamics adds robustness, while the stepwise nature of the reconfiguration maneuver provides many safe-hold points for verification regardless of transient dynamics. The focus on kinematic constraints lends itself well to Udwadia and Kalaba's technique for generating equations of motion. This work details the augmentation of the Udwadia-Kalaba equations with quaternion states and Euler's equation for fully 3D rigid body motions, as well as the development of a simulation environment and computational tools for exploring sequential-equilibrium reconfigurations.

Nomenclature

$\mathbb{0}_n$	=	matrix of zeros (subscripts indicate dimensions; square if only one subscript)
$\mathbb{1}_n$	=	identity matrix (subscript indicates dimension)
A	=	constraint matrix
a	=	acceleration matrix (equal to $\ddot{x}$ in the absence of constraints)
^{B}	=	body B frame of reference
^{C}	=	body C frame of reference
b	=	constraint matrix
F	=	system applied force matrix
F_B	=	applied force matrix for body B
$\tilde{F}_B$	=	intermediate force matrix for body B
$\boldsymbol{f}_B$	=	applied force vector on body B at center of mass
$\boldsymbol{I}_B$	=	inertia dyadic of body B about center of mass
M	=	system mass matrix
M_B	=	mass matrix for body B
$\tilde{M}_B$	=	intermediate mass matrix for body B
m	=	number of constraint equations
^{N}	=	inertial frame of reference
n	=	number of position and orientation states (number of elements in x)
$\boldsymbol{p}_{BC}$	=	vector from body B center of mass to joint connecting body B to body C
$^N Q^B$	=	direction-cosine matrix rotation from frame B to N
$^N q^B$	=	quaternion rotation from frame B to N
$\boldsymbol{r}_B$	=	center-of-mass position of body B
T	=	transformation matrix relating quaternion derivative to angular velocity

[1] Graduate Research Assistant, Department of Mechanical and Aerospace Engineering, 127 Upson Hall, Student Member AIAA.
[2] Assistant Professor, Department of Mechanical and Aerospace Engineering, 212 Upson Hall, Member AIAA.

t = time
U = potential energy function
x = matrix representing a point in configuration space corresponding to the multibody system position and orientation state
$\boldsymbol{\tau}_B$ = applied torque vector on body B about center of mass
$\boldsymbol{\omega}^{B/N}$ = angular velocity vector of reference frame B with respect to frame N

I. Introduction

SPACECRAFT architectures capable of autonomous reconfiguration face a major hurdle in implementation: in-orbit reconfiguration of such modular spacecraft systems is a challenging problem in controls and dynamics. Often, proposed solutions to this problem involve a combination of multibody dynamics, multivariable controls, docking hardware and algorithms, state estimation, and the relative orbital dynamics of formation flight, expressed as a tracking problem.[1,2,3,4,5,6] These approaches incorporate interactions between many vehicles, sensors, and actuators, and thus may be both computation- and power-intensive, with many potential points of failure. With the goal of adding robustness, determinacy, and power savings to the reconfiguration process, we have proposed that modular spacecraft designs include the capability to alter their kinematic properties.[7] After each such alteration, the multibody system would evolve dynamically due to the presence of ambient forces in the space environment, such as gravity gradients, solar pressure, and planetary magnetic fields, towards a stable equilibrium. From this stable equilibrium, the multibody system can make further changes to its kinematics and passively evolve again. A reconfiguration maneuver in this framework is thus composed of a sequence of natural, dissipative motions towards passive equilibria of the multibody system. In this manner, spacecraft composed of many modules can execute complex but failure-robust reconfiguration maneuvers with little to no control computation or actuation. Any required computations can be performed offline with common multibody dynamics techniques, and operators on the ground can verify the system state while it is paused at any "safe step" intermediate equilibrium.

There is a parallel between this reconfiguration concept and mechanical deployments in which the potential energy provided by a spring causes a joint to move to a passive dynamic equilibrium. In general, such an approach to reconfiguration may apply to any modular spacecraft system in which kinematic joints link the modules; however, it is especially relevant to systems with modules already connected by force fields through one of several enabling technologies. Such systems include Coulomb-tether formations[8] and Electromagnetic Formation Flight,[9] though these approaches involve active control strategies, reducing the benefits of reconfiguration through passive dynamics. Alternatively, modular space systems linked with magnetic flux pinning are passively stable non-contacting systems with inter-module separation ranges up to tens of centimeters.[10,11,12] These systems blur the distinction between modular systems of docked spacecraft and formation flying spacecraft,[13] with varied applications ranging from particulate solar sails[14] to sparse-aperture telescopes.[15] Magnetic flux pinning is an interaction between type II high-temperature superconductors (HTSCs) and magnetic fields in which sufficiently strong magnetic fields penetrate the superconducting material. The applied magnetic field lines become trapped on these impurities in the HTSC; supercurrents excited by the applied field oppose any motion of the flux lines away from such "pinning" sites.[16] A simple (and effective, for small motions) model of a flux-pinned magnet-superconductor pair connects the two bodies by a multiple-degree-of-freedom (DOF) spring and damper.[17,18] The linear stiffness of a flux-pinned magnet-superconductor pair depends on the separation of the two objects and can exceed hundreds of newtons per meter.[10,11]

Flux pinning is ideal for space assembly applications. It can create passively stable 6DOF equilibria among multiple bodies in space since the magnetic field of the supercurrents depends on the three-dimensional positions, orientations, and motions of flux-pinned magnets. In addition, this effect does not require power. As long as the HTSC material remains in its superconducting state (that is, below its critical temperature: $T_c \approx$ 80-90 K for common superconductors), it pins magnetic flux. No voltage need be applied to the superconductor, and no actuation of the magnet is required. The prospect of passive stability following any of several power-, control-, or propulsion-related failures is an attractive possibility for any spacecraft for which fault tolerance is expected. Furthermore, the stiffness and damping properties of the flux-pinning interaction depend on the shape of the magnetic field pinned to the superconductor. Thus, shaping a magnetic field pinned to a HTSC introduces or removes stiffness, creating a reconfigurable, non-contacting, kinematic mechanism.[12] Other shaping of the magnetic fields, along with exploitation of rigid-body dynamics, gravity gradient, and other ambient forces, may change the stability of the equilibrium points of these mechanisms. In addition, cooling and warming the superconductors is a means to toggle inter-module interfaces. Control of a reconfiguration maneuver for such a system therefore takes the form of specified magnetic field geometries at each interface, to introduce or stiffen appropriate kinematic degrees

of freedom, with accompanying magnetostatic, electrostatic, gravitational, or Coriolis forces that cause the system to passively "fall" towards a desired equilibrium in configuration space. Multiple steps between sequential equilibria allow the system to reach many possible configurations. In these non-contacting systems, spacecraft assembly can be executed as a similar sequence, with modules falling into 6DOF basins of attraction.

In 2009, members of our research group demonstrated a simple flux-pinned kinematic mechanism in a NASA microgravity program.[19] The demonstrations, with CubeSat mockups, showed that flux pinning can be implemented on the nanosatellite scale and that vehicles equipped with flux-pinned interfaces can form non-contacting revolute joints, with stiffness in all but one degree of freedom. Future microgravity flights will demonstrate the autonomous assembly of flux-pinned systems and their robustness to sensing and control failures. Simultaneously, we are developing an air-levitated laboratory testbed to examine small satellite reconfiguration maneuvers and algorithms.[20]

This paper reports the development of a simulation environment for exploring space system reconfiguration as a sequence of passive dynamical evolutions with chosen sets of kinematic constraints. These simulations are based on the formulation of equations of motion from Udwadia and Kalaba, because of the ease with which that formulation accounts for kinematic constraints.[21] Section II describes the sequential-equilibrium multibody spacecraft reconfiguration concept at a high level. Section III then develops equations of motion, with the Udwadia-Kalaba technique augmented by quaternion states and Euler's equation for rigid body dynamics, for implementation in simulations. Using these simulations, Section IV explores possible reconfigurations of example spacecraft systems and develops methods to identify reconfiguration maneuvers for general systems. Furthermore, this simulation environment provides tools for the analysis of the air-levitated testbed and microgravity flight experiments, and suggests conclusions about power usage during reconfiguration maneuvers and dynamic stability of reconfiguring systems.

II. The Sequential-Equilibrium Reconfiguration Concept

A single point in an n-dimensional configuration space represents the physical configuration of a multibody system with n degrees of freedom. The configuration space may take the form of ordered n-tuples of, for example, joint angles and offsets.[22] Configuration space is thus related, but not identical, to state space. In Hamiltonian dynamics, the configuration space often appears embedded in higher-dimensional Euclidian space and weighted by the kinetic energy of the system; this weighted surface is called the configuration manifold and represents all the possible trajectories of a physical system.[23]

The architecture of a reconfigurable space system in this paradigm includes kinematic constraints, defining the locus of allowable points in configuration space that the system may occupy. In Hamiltonian language, the kinematic constraints determine the shape and dimensionality of the configuration manifold embedded in higher-dimensional space. In this treatment, kinematic constraints appear as boundaries of the configuration space. The system may move continuously from point to point in configuration space as both external and internal forces act on the system, in accordance with the laws of motion. An important point for this reconfiguration concept is that specified alterations of the kinematic constraints are part of the control effort on the multibody system. That is, some of the control laws acting on the system involve changing the allowed trajectories in configuration space so that the system naturally evolves towards a desired configuration.

Given a multibody system represented by a point in configuration space, let us now introduce force fields to augment its dynamics with a potential function. This potential function is a scalar value associated with each point in configuration space, resulting from an application of internal or external forces or torques to the system—for instance, gravity gradient, interactions between a dipole on the spacecraft and a planetary magnetic field, solar radiation pressure, electromagnetic fields interacting between multibody spacecraft modules, or springs connecting spacecraft bodies. Now, depending on the shape of the potential function, there will be dynamic equilibria, represented by minima or "wells" in the potential, in configuration space. The system will naturally move towards these equilibria and, assuming that the system is dissipative, will settle into the potential well in steady state. From the equilibrium, a new set of kinematic constraints and a new potential function could drive the system to evolve to a different equilibrium. The space system proceeds from one configuration to the next in a "stepping-stone" fashion until it reaches a target configuration. The following three steps identify the possible reconfiguration maneuvers a system may undergo:

1. Determine, from the possible kinematic constraints on the system, the allowed trajectories of the system in configuration space.
2. Set up a potential to create a stable equilibrium at a location in configuration space. Allow the system to evolve dynamically in simulation, settling into the resulting potential well.

3. If necessary, identify any newly allowed trajectories in configuration space and repeat the first two steps to move the system to another point in configuration space.

The applied control input at each discrete step in this process consists of a collection of the assigned kinematics of the multibody system and the potential $U(x)$ from the applied force fields. At each stepping-stone configuration, the choice of kinematics and potential must be one of the allowable selections associated with that point in configuration space. Such selections will, in general, depend on the proximity of the various bodies and the properties of the joints in question. Similarly, the selection of $U(x)$ must be a member of the finite set of possible functions related to the spacecraft capabilities and environment. Some potential functions, such as those due to gravity or rigid-body dynamics, will always be present.

The terminology of hybrid automata[24] applies to this description in a straightforward manner. The continuous modes of the automaton are each set of dynamics while the system kinematics remain constant; that is, the dynamics of the system at any configuration-space equilibrium and during the dissipative transition to that equilibrium. The possible collections of kinematics are the guards enabling discrete transitions. The invariants that cause the automaton to perform a discrete transition are conditions that the current configuration (represented by a state space vector x) must be at a potential minimum, $x_{eq} = (x|U(x) = \min U)$. The control strategy in this paper involves manipulating the invariants and guards to guide the hybrid execution of the automaton to a continuous mode with a desired equilibrium configuration x_{target}.

As an illustration of the process, let us consider a system consisting of two bodies in free space, with one of two possible joints linking them together. The bottom plane in Figure 2 represents a two-dimensional configuration space for these bodies; for example, the separation between their centers of mass and their relative angle about an arbitrary axis. Control over this system consists of the choice of joint and the application of an arbitrary force field to establish a potential function along the line of allowed configurations. The system starts at Point 1 in configuration space, with the kinematic constraint that the system must move along the blue dotted line in configuration space and a potential energy along that line given by the height of the blue curve (Figure 2). The presence of a potential minimum will move the system from Point 1 to Point 2. This process may involve transient dynamics; the reconfiguration sequence does not proceed further until the system has reached steady state. If the new configuration is not the desired final configuration of the system x_{target}, another selection of kinematic constraints (such as the green dotted line) and potential function may drive the system to move to yet another configuration, such as from Point 2 to Point 3. Figure 1 shows a possible time history of the system evolution.

There are several important points illustrated by this example. The first is that the

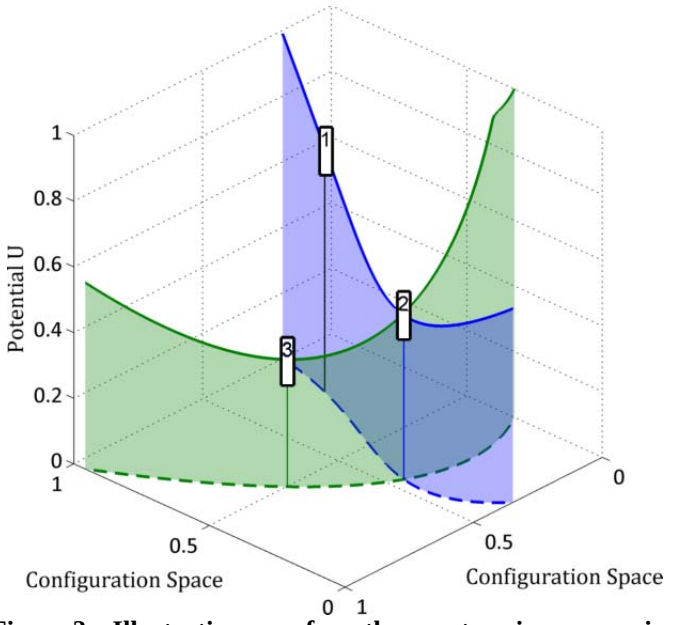

Figure 2. Illustration of the stepwise passive reconfiguration concept in a system with two possible degrees of freedom augmented with potentials.

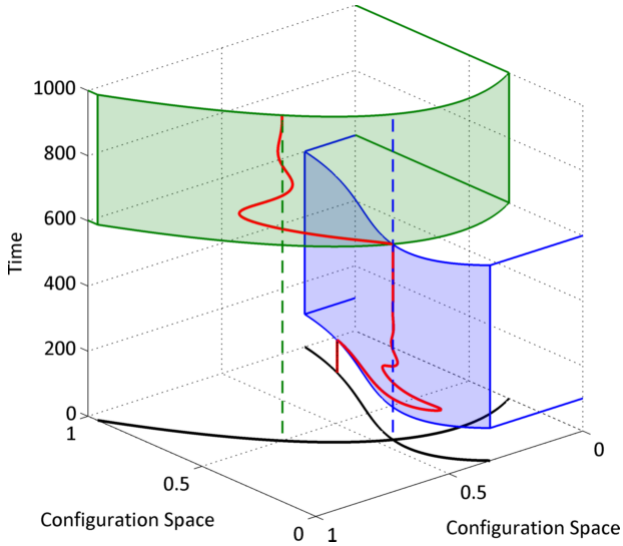

Figure 1. Sample time history of the system from Figure 2. The control input changes at t = 100 s and again at t = 600 s, triggering discrete transitions in the hybrid automaton.

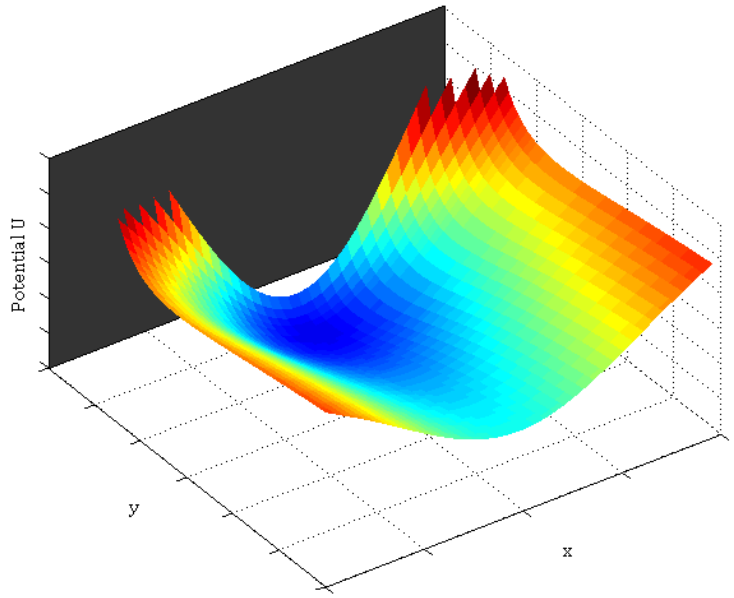

Figure 3. Illustration of the magnetic potential well linking a flux-pinned magnet and superconductor. The superconducting plane is shaded.

system cannot reach Point 3 directly from Point 1, given the possible system kinematics. In a more complex system, kinematic constraints may not change only in character but also appear and disappear, so some configurations are certain to be impossible to reach from other configurations and intermediate steps will be necessary. This situation is the case in a system that engages and disengages some of its joints as the component bodies come close to or separate from one another. A second point is that this control strategy does not require any sensing, computation, or feedback actuation of the system while it is between equilibria in configuration space. This concept requires only knowledge of the initial and final configurations for each step in the process, as long as the intermediate dynamics meet any safety and robustness criteria, such as collision avoidance, which may be verified in simulation before the maneuver begins. It is a hybrid control scheme in which the continuous-time dynamics of the system are less relevant than the configuration space points at which the system dynamics change. On a space system with limited computation capabilities, determination of the locus of possible reconfiguration sequences may occur on the ground and either be transmitted on an as-needed basis or stored in spacecraft memory as a compact lookup table. The on-board reconfiguration controller need only know the desired configuration and determine a possible set of intermediate steps.

This control architecture is based on a large set of equilibria in configuration space, and the identification of reachable equilibria from the current system configuration. Graph theory provides a convenient language to describe the equilibria and the control inputs necessary to move the spacecraft system from one to another. In this paradigm, each reconfigurable space system has an associated "reconfiguration graph." The vertices of the reconfiguration graph represent each of the possible passively stable potential wells of the system in configuration space x, while the directed arcs represent the collections of kinematics and potentials that take the system from one configuration x to another x'. For application in a spacecraft system, the graph will be constructed offline according to the three-step process described above. Important questions for reconfiguration control, such as which configurations are reachable from a given initial configuration and which configurations, if any, are "sinks" from which the system cannot proceed further, will be answered from this graph. A well-constructed reconfiguration graph inherently prevents transient dynamics that include unsafe behaviors such as collisions, as those transient dynamics could be identified in simulation and eliminated from the graph. Such a graph theoretical approach highlights how this reconfiguration paradigm allows spacecraft or spacecraft operators to concentrate on reconfiguration tasks from a high level, relegating the low-level evolution of the system from one configuration to another to passive physics.

The feature of flux pinning that makes it particularly attractive to this approach to reconfiguration is that it provides a means to establish stable potential wells in all six degrees of freedom. Figure 3 shows a sketch of the potential well binding a flux-pinned permanent magnet to a superconducting plane in translation space, $U(x, y)$. A frozen-image model of flux pinning generated the data for this plot.[10,25] If the magnet does not have an axisymmetric field, similar potential wells keep the magnet stably positioned with respect to the superconductor in the remaining four degrees of freedom as well. Establishing such stable potential wells is critical to enabling reconfiguration with no active control, as it is the passive stability of these wells that allows this control strategy to ignore the continuous-time dynamics of the system when it moves from point to point in configuration space.

III. Formulation of Udwadia and Kalaba's Fundamental Equation with Quaternion States

A. Derivation of General Equation of Motion with Quaternion States

Udwadia and Kalaba give an algorithm for finding equations of motion,[21] for systems with constraints that can be expressed in terms of the second derivative of the system state x (a vector of accelerations):

$$A(x, \dot{x}, t)\ddot{x} = b(x, \dot{x}, t). \tag{1}$$

The state vector x contains all n position and orientation states of the entire multibody system, and the matrices A and b ($m \times n$ and $m \times 1$, respectively, with elements that may depend on the system state and time) express the m constraint equations. In the presence of applied forces F such that

$$F = Ma, \tag{2}$$

where M is the system mass matrix and a is the acceleration vector *in the absence of all constraints* (1) (in other words, F includes no constraint forces), the following expression is the equation of motion of the system:

$$M\ddot{x} = F + A^{\mathrm{T}}(AM^{-1}A^{\mathrm{T}})^{+}(b - AM^{-1}F). \tag{3}$$

The superscript $^{+}$ indicates a Moore-Penrose matrix pseudoinverse. Eq. (3) is one of several possible expressions of Udwadia and Kalaba's Fundamental Equation. It can be evaluated analytically, by hand or in a symbolic computation environment, or numerically at every time step of an integration.

Evaluating the prospects of the proposed reconfiguration concept requires a simulation environment that can accommodate bodies with arbitrary positions and orientations in six degrees of freedom (6DOF). In the process of computing a reconfiguration maneuver as a sequence of dynamical evolutions, there are not necessarily any conditions on the orientation of each body in an arbitrary multibody system at the end of each evolution. Therefore, we wish to avoid formulating equations of motion that may be susceptible to singularities if the bodies take certain orientations, such as those associated with Euler angles. To this end, the state of each body B (in an inertial frame) is expressed as its center of mass position and quaternion attitude:

$${}^{N}x_{B} = \begin{bmatrix} {}^{N}r_{B} \\ {}^{N}q^{B} \end{bmatrix}. \tag{4}$$

${}^{N}q^{B} = \begin{bmatrix} \left({}^{N}q^{B}_{123}\right)^{\mathrm{T}} & {}^{N}q^{B}_{4} \end{bmatrix}^{\mathrm{T}}$ denotes the quaternion relating the rotation from the reference coordinates of body B to an inertial coordinate system N, with superscripts analogous to the notation for direction-cosine matrices, ${}^{N}Q^{B}$.

The equation of unconstrained motion in the position states is straightforward:

$${}^{N}f_{B} = m_{B}\,{}^{N}\ddot{r}_{B} \tag{5}$$

However, in order to account for rigid-body dynamics in 6DOF, Eq. (2) must include not only the force $\boldsymbol{f}_B$ on the body center of mass but also terms due to Euler's equation for rigid body motion with a torque on body B about its center of mass,

$$\boldsymbol{\tau}_{B} = \boldsymbol{I}_{B} \cdot \left(\overset{B}{\boldsymbol{\omega}}{}^{B/N}\right) + \boldsymbol{\omega}^{B/N} \times \boldsymbol{I}_{B} \cdot \boldsymbol{\omega}^{B/N}. \tag{6}$$

In B, the angular velocity and derivative of the angular velocity can be expressed in terms of the quaternion elements. This approach allows the portion of Eq. (2) dealing with rotational states of each body to be recast with an effective mass matrix and effective force. Suppressing the superscripts on ${}^{N}q^{B}$ for brevity, the transformation between angular velocity and quaternion derivative is:

$$
\begin{aligned}
{}^{B}\omega^{B/N} &= 2[(-q_{123}^{\times} + q_4\mathbb{1}_3) \quad -q_{123}]q \\
{}^{B}\omega^{B/N} &= T(q)q
\end{aligned}
\tag{7}
$$

with a superscript $^{\times}$ denoting the 3×3 skew-symmetric cross-product matrix form of a 3×1 matrix and $T^{\mathrm{T}}T = TT^{\mathrm{T}} = \mathbb{1}_3$. Euler's equation then becomes

$$
{}^{B}I_B(\dot{T}\dot{q} + T\ddot{q}) = {}^{B}\tau_B - (T\dot{q})^{\times}\,{}^{B}I_B(T\dot{q}) \tag{8}
$$

$$
{}^{B}\tau_B - (T\dot{q})^{\times}\,{}^{B}I_B(T\dot{q}) - {}^{B}I_B\dot{T}\dot{q} = {}^{B}I_BT\ddot{q} \tag{9}
$$

This expression is analogous to Eq. (5), but the matrix ${}^{B}I_BT$, which serves as the mass matrix, is 3×4. Eq. (3) requires a square system mass matrix; so, we pre-multiply Eq. (9) by the transpose of the transformation matrix T^{T}:

$$
\begin{aligned}
T^{\mathrm{T}}\,{}^{B}\tau_B - T^{\mathrm{T}}(T\dot{q})^{\times}\,{}^{B}I_B(T\dot{q}) - T^{\mathrm{T}}\,{}^{B}I_B\dot{T}\dot{q} &= T^{\mathrm{T}}\,{}^{B}I_BT\ddot{q} \\
\tilde{F}_B(q,\dot{q},\tau_B) &= \tilde{M}_B(q)\ddot{q}
\end{aligned}
\tag{10}
$$

As a check, we note that

$$
\frac{1}{2}\dot{q}^{\mathrm{T}}\tilde{M}_B\dot{q} \tag{11}
$$

gives the correct rotational kinetic energy expression for the body.

The effective force and mass matrices for body *B* are, therefore,

$$
F_{B,eff} = \begin{bmatrix} {}^{N}f_B \\ \tilde{F}_B(q,\dot{q},\tau_B) \end{bmatrix} \tag{12}
$$

$$
M_{B,eff} = \begin{bmatrix} m_B\mathbb{1}_3 & \mathbb{0}_{3\times4} \\ \mathbb{0}_{4\times3} & \tilde{M}_B(q) \end{bmatrix} \tag{13}
$$

for use in Eq. (3). The effective force matrix for the entire system consists of a stack of the effective force matrices of each body, and the system effective mass matrix is comprised of a block matrix of each body's effective mass matrix. $M_{B,eff}$ is rank-deficient because of the transformation from three-element angular velocity vectors to four-element quaternion derivatives. Fortunately, Udwadia and Phohomsiri[26] developed a form of Eq. (3) that handles singular mass matrices and redundant coordinates,

$$
\ddot{x} = \begin{bmatrix} (\mathbb{1} - A^{+}A)M_{eff} \\ A \end{bmatrix}^{+} \begin{bmatrix} F_{eff} \\ b \end{bmatrix}, \tag{14}
$$

provided that the constraint matrix A includes any constraints between redundant coordinates. In the case of quaternion states, this includes the second derivative of the constraint that the norm of any quaternion must equal 1,

$$
\begin{aligned}
&\frac{\mathrm{d}^2}{\mathrm{dt}^2}(q^{\mathrm{T}}q = 1) \\
&2q^{\mathrm{T}}\ddot{q} + 2\dot{q}^{\mathrm{T}}\dot{q} = 0.
\end{aligned}
\tag{15}
$$

This is the form of Eq. (3) that we have implemented in a set of MATLAB toolbox functions.

B. Constraint Matrices for Joints with Quaternion States

The constraint matrix corresponding to a joint connecting, for example, bodies *B* and *C* must conform to the following template:

$$\begin{bmatrix} \cdots & A_{r_B} & A_{{}^N q^B} & \cdots & A_{r_C} & A_{{}^N q^C} & \cdots \end{bmatrix} \begin{bmatrix} \vdots \\ \ddot{r}_B \\ {}^N\ddot{q}^B \\ \vdots \\ \ddot{r}_C \\ {}^N\ddot{q}^C \\ \vdots \end{bmatrix} = b \tag{16}$$

A has zeros in all other elements. For example, if a spherical joint connecting bodies B and C is located at the point $\boldsymbol{p}_{BC}$ from body B's center and $\boldsymbol{p}_{CB}$ from body C's center, the second derivative of the single vector constraint

$$\boldsymbol{r}_B + \boldsymbol{p}_{BC} = \boldsymbol{r}_C + \boldsymbol{p}_{CB} \tag{17}$$

gives the constraint matrix elements, with full superscripts,

$$\begin{aligned} A_{r_B} &= \mathbb{1}_3 \\ A_{{}^N q^B} &= \left({}^N Q^B \, {}^B p_{BC}\right)^\times T_B \\ A_{r_C} &= -\mathbb{1}_3 \\ A_{{}^N q^C} &= -\left({}^N Q^C \, {}^C p_{CB}\right)^\times T_C \\ b &= ((T_C \dot{q}_C)^\times)^2 \, {}^N Q^C \, {}^C p_{CB} + \left({}^N Q^C \, {}^C p_{CB}\right)^\times \dot{T}_C \dot{q}_C - ((T_B \dot{q}_B)^\times)^2 \, {}^N Q^B \, {}^B p_{BC} - \left({}^N Q^B \, {}^B p_{BC}\right)^\times \dot{T}_B \dot{q}_B. \end{aligned} \tag{18}$$

Similarly, one expression for the constraint matrices for a revolute joint or hinge with its rotation axis aligned with a unit vector $\hat{\boldsymbol{a}}$ that is fixed on the body B can be derived from Eq. (17) along with the requirement that $\hat{\boldsymbol{a}}$ must be an eigenvector of the direction-cosine matrices ${}^N Q^B$ and ${}^N Q^C$, with eigenvalue 1:

$$\begin{aligned} A_{r_B} &= \begin{bmatrix} \mathbb{1}_3 \\ \mathbb{0}_3 \end{bmatrix} \\ A_{{}^N q^B} &= \begin{bmatrix} \left({}^N Q^B \, {}^B p_{BC}\right)^\times T_B \\ \left({}^N Q^C\right)^T \left({}^N Q^B \, {}^B \hat{a}\right)^\times T_B \end{bmatrix} \\ A_{r_C} &= -\begin{bmatrix} \mathbb{1}_3 \\ \mathbb{0}_3 \end{bmatrix} \\ A_{{}^N q^C} &= -\begin{bmatrix} \left({}^N Q^C \, {}^C p_{CB}\right)^\times T_C \\ \left({}^N Q^C\right)^T \left({}^N Q^B \, {}^B \hat{a}\right)^\times T_C \end{bmatrix} \\ b &= \begin{bmatrix} ((T_C \dot{q}_C)^\times)^2 \, {}^N Q^C \, {}^C p_{CB} + \left({}^N Q^C \, {}^C p_{CB}\right)^\times \dot{T}_C \dot{q}_C - ((T_B \dot{q}_B)^\times)^2 \, {}^N Q^B \, {}^B p_{BC} - \left({}^N Q^B \, {}^B p_{BC}\right)^\times \dot{T}_B \dot{q}_B \\ \left({}^N Q^C\right)^T \left(((T_C \dot{q}_C)^\times)^2 - 2(T_C \dot{q}_C)^\times (T_B \dot{q}_B)^\times - \left(\dot{T}_B \dot{q}_B - \dot{T}_C \dot{q}_C\right)^\times\right) {}^N Q^B \, {}^B \hat{a} \end{bmatrix}. \end{aligned} \tag{19}$$

The second derivatives of other joint constraint equations generate other constraint matrix elements in the same manner. A simple vertical stack of these constraint matrices for each joint accounts for many joints in a multibody system. This system constraint matrix can include nonholonomic and redundant constraints when implemented for simulation. For example, the revolute constraint matrices of Eq. (19) have six equations representing only five constraints.

IV. Simulation of Sequential Multibody Reconfiguration

An object-oriented implementation of the constraint equation and equation of motion generating algorithm from Section III in MATLAB provides an intuitive and extensible simulation environment. The key classes of this simulation environment toolbox are:

- *Body objects*, which store the physical properties and track the position and quaternion state of a rigid body, as well as providing graphical representations of bodies for animation;
- *Joint objects*, which provide the constraint matrices (e.g. Eq. (18) or (19)) between connected bodies;

- *Force objects*, which provide force and torque functions on bodies;
- *Sensor objects*, which are attached to bodies and can halt simulations of multibody motion when they come into proximity of one another; and
- *Multibody objects*, which act as containers for all the above classes, specify information relevant to entire systems such as potential energy functions, use Eqs. (12), (13), and (14) with MATLAB's ode45 function to solve equations of motion, and include various plotting and animation functions for analyzing the motion of multibody systems.

These toolbox functions are available on the Internet at http://www.spacecraftresearch.com/flux. The implementation easily accommodates simple multibody mechanisms, and provide the means to develop an algorithm to construct the reconfiguration graph of a multibody system with switchable kinematic constrains through direct simulation, as Section II describes.

The algorithm proceeds as follows:

1. Set up bodies in initial configuration and set initial potential energy.
2. Place sensor objects at locations on bodies where joint connections are possible.
3. Add the current configuration of the bodies, represented as a single node, to a graph object. Add this node to a list of nodes that require processing.
4. Loop through each node in the processing list.
   - 4.1. Enumerate all possible combinations of joints (where compatible sensors are in proximity) and potential energy functions with this configuration of bodies.
   - 4.2. Loop through all combinations of joint set and potential energy selections.
     - 4.2.1. Place selected joints on bodies and set multibody system potential energy to the current selection.
     - 4.2.2. Simulate the motion of the multibody system, until either the system reaches equilibrium or two sensors come into proximity.
     - 4.2.3. Check the configuration of the bodies after simulation against safety criteria. If safety criteria are violated (for example, if one of the bodies separates from the rest or bodies collide during simulation), terminate this iteration of the loop.
     - 4.2.4. Check the configuration of the bodies after simulation against the configurations represented by all extant nodes in the graph. If the configuration does not match any existing nodes, place it in a new node and add it to the graph.
     - 4.2.5. Add a directed edge to the graph, representing the transition between the node being processed and the newly generated node. This edge contains the joint set and potential energy selection of this iteration.
   - 4.3. Remove the processed node from the processing list.
5. Save the reconfiguration graph of the system.

This algorithm takes the brute-force approach of enumerating all possible joint layouts and potential energies, and simulating the resulting multibody dynamics to identify equilibrium positions. Given enough time and computing power, it will construct the entire reconfiguration graph for an arbitrarily complex system.

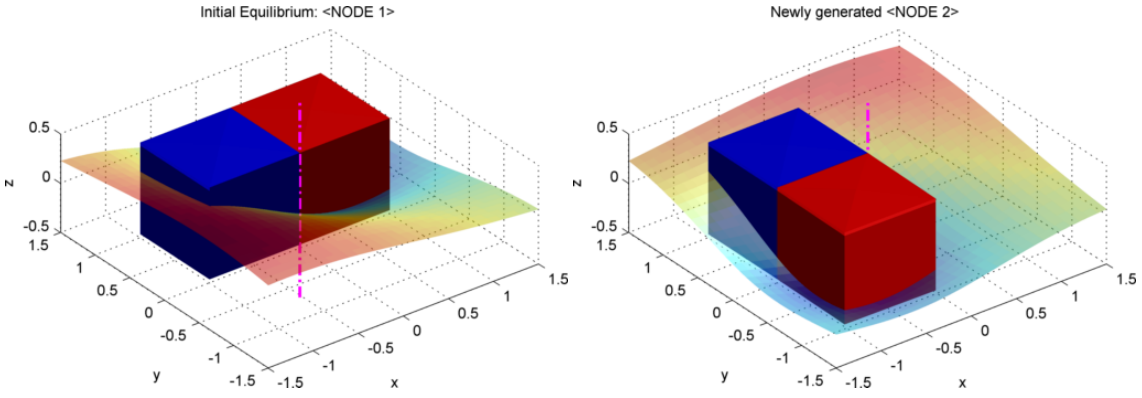

Figure 4. First reconfiguration example: multibody system equilibria at two nodes in the reconfiguration graph. The dashed line indicates the rotation axis of a revolute joint. The shaded surface's height shows the potential energy as a function of *x* and *y* position of the bodies. See text for full description.

A. Simulation of Two-Equilibrium Laboratory Demonstrations

Consider the following reconfiguration example, which reproduces the results from laboratory demonstrations with two flux-pinned, CubeSat-sized spacecraft mockup modules on an air table[20] and a NASA microgravity flight.[19] One cube-shaped module (blue in Figure 4) is inertially fixed, while the other (red) is attached to the first module by a hinge with is rotation axis aligned with the bodies' z axes. Sensor objects detect when the cubes' faces align and terminate simulation so that the cubes "lock" together in these positions. There are two possible potential energy functions, with a potential well either in the positive x or negative y direction from the center of the blue cube. Selection of one potential energy function or the other determines the system's equilibrium. The algorithm successfully computes the reconfiguration graph of this system, which consists of two nodes representing the two configurations in Figure 4 connected by two directed edges representing each of the two potential energy selections. In the physical systems, combinations of magnets and electromagnets realize these potential energies.

This system is entirely passive during the reconfiguration from one equilibrium to another. A plot of the system's total energy appears in Figure 5. Total energy decreases because there is some dissipation in the multibody system to encourage numerical stability. During the motion, the system does not use power except that which is necessary to maintain the potential energy functions. In the case of the laboratory demonstrations, there is constant power supplied to electromagnets during the motion. However, the potential energy functions could also be realized by permanent magnets that move or rotate to change between the two potentials. In that case, at the point when a new reconfiguration maneuver begins, the system must perform work equal to at least the difference between the value of the previous potential energy and the value of the new potential energy at the same state of the system. For the identical potential wells of Figure 4, this change in energy is the difference between the values of the potential energy at the beginning and end of the time series shown in Figure 5. For other systems, such power expenditures must be considered against the power consumed by a feedback control system to determine which approach is advantageous.

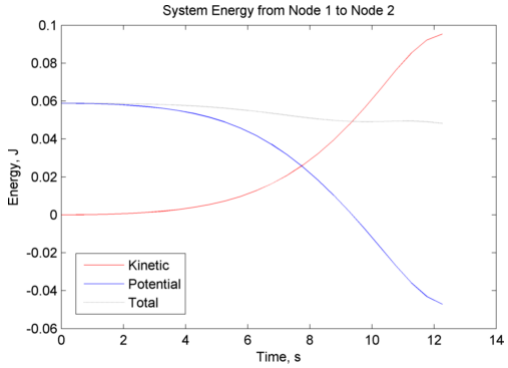

Figure 5. System energy as a function of time.

B. Planetary Imaging Mission

A second example of a reconfigurable system with a kinematically defined reconfiguration graph is an innovative planetary imaging mission consisting of a spacecraft with four identical modules. Each module has a suite of cameras or other instruments, a set of possible revolute or fixed joint locations, and the capability to energize or reorient magnetic fields to change the potential energy of the spacecraft. Figure 6 shows the initial configuration of the spacecraft, with possible joint sites marked. Each joint site can be fully free, fully fixed, or a revolute joint. A sketch of part of the spacecraft's reconfiguration graph, as identified by our simulation algorithm, appears in Figure 7.

Each configuration of this spacecraft serves a mission purpose. For example, the initial configuration is appropriate for launch and for injection into a transfer orbit to the target planet. The configuration in the center of Figure 7 is a compact arrangement of modules with cameras and instruments facing slightly outward, giving the spacecraft wide-angle imaging capabilities for context. This configuration is also a stepping stone to several of the other possible configurations. For example, from this compact shape, the spacecraft can spread into a linear formation that allows its cameras to sweep across large swaths of the planetary surface. This layout may efficiently acquire a planetary map or cover the same ground with multiple instruments; or, if the imaging fields overlap, it may acquire stereo images on the same orbital pass. The spacecraft configurations on the left and right of Figure 7 each have one module separated out from the main body of the spacecraft. Such a configuration may be useful if the separated module is faulty and a new module must replace it.

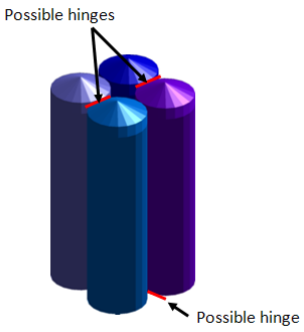

Figure 6. Second reconfiguration example: initial system configuration and possible joint layout.

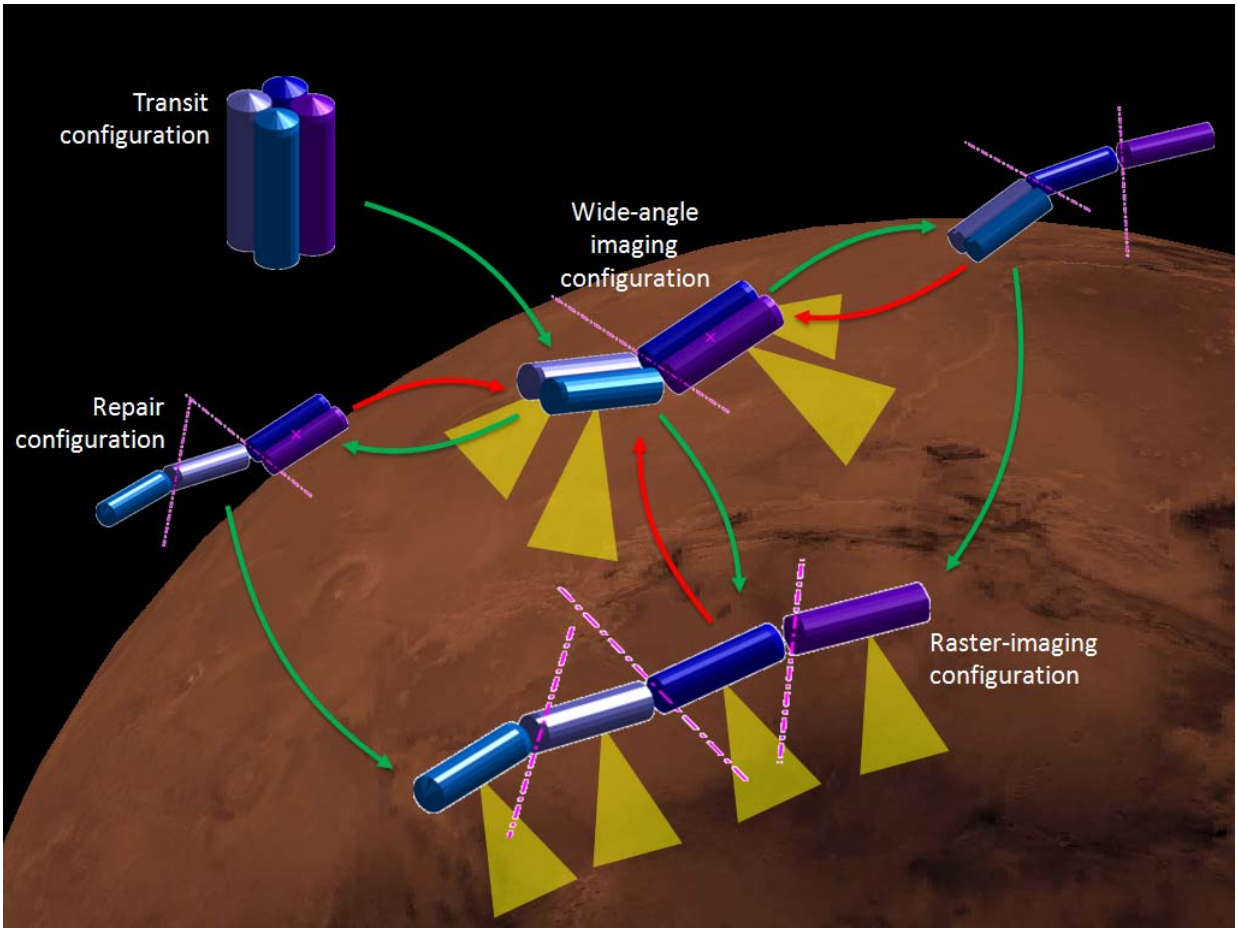

Figure 7. Partial reconfiguration graph for a hypothetical planetary imaging mission. Dashed lines indicate hinges. See text for full description.

Each configuration of the spacecraft is a dynamic equilibrium, and each transition is free of collisions. A software or control problem on the spacecraft therefore results in one of several relatively benign failure modes that do not involve hardware damage. If a control failure occurs when the spacecraft is at an equilibrium configuration, then the spacecraft remains in that configuration. If, however, the failure occurs while the spacecraft is carrying out a maneuver, then the system continues to move until it reaches dynamic equilibrium. In either case, the system remains passively stable, with kinematic constraints that prevent motions with any danger of collisions. Only a hardware failure of the joints themselves could pose a danger to the spacecraft.

In this system, ambient forces drive some of the transitions between nodes in the reconfiguration graph. The green arrows in Figure 7 represent transitions accomplished when gravity gradient, a force that tends to pull the modules apart, provides the potential energy function on the spacecraft. The red arrows represent transitions for which the spacecraft must provide at least some of the potential energy, by energizing electromagnets, for example. Depending on the specific sequence of reconfigurations, the spacecraft might use very little power; or it might perform power-intensive maneuvers very infrequently.

Figure 8 displays some qualitative energetics for this system as it performs a sequence of three reconfigurations, from transit configuration to wide-angle imaging, then to raster imaging, and finally back to the wide-angle imaging configuration, in the presence of a small amount of dissipation. The first two steps in the sequence are composed of entirely passive motions, so the spacecraft uses no power to drive or control its motion. However, the spacecraft initiates its transition from the wide-angle imaging configuration to the raster-imaging configuration by changing its kinematic joint layout, so there is a brief use of on-board power in the middle of this otherwise passive sequence. A more prominent spike in power usage occurs at the beginning of the reconfiguration from raster-image form to the wide-angle imaging configuration. This spike is due not only to selecting the proper joint kinematics but also to raising the potential energy of the system to drive the reconfiguration back to the wide-angle imaging layout. Energy losses in, e.g., electromagnets continue to consume power during the subsequent motion. Again, a trade study must

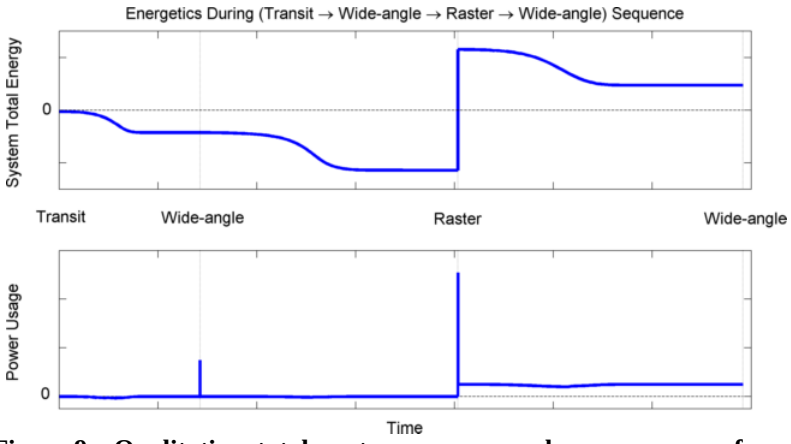

Figure 9. Qualitative total system energy and power usage for a sample reconfiguration sequence of the planetary imaging mission. See text for full description.

compare the power usages of this reconfiguration method and one involving feedback control and actuation in the context of this mission.

One of the strengths of this reconfiguration methodology is that it can identify opportunities for emergent behaviors. For example, the different arrangements of cameras in Figure 7 may allow the spacecraft to function as a set of filter masks for interferometry that emphasizes different spatial scales depending on the configuration. In addition, the enumeration of all possible equilibrium configurations of the space system may identify configurations that enable otherwise unanticipated functionality, or it may identify sequences of reconfigurations that reach a desired end state in some advantageous way. The prospect for such emergent behaviors increases with system complexity, as the algorithm enumerates many more possible transitions.

V. Conclusion

The reconfiguration of multibody spacecraft systems in orbit will be an important part of future space development. Reconfiguration is related to the in-orbit docking, assembly, repair, and refurbishment of high-value systems and provides an avenue for small, responsive space systems to perform a wide range of functions and meet many different mission needs. Low-power, robust approaches to space system reconfiguration will allow many more future space systems to take advantage of these capabilities. These systems may include applications from large-aperture, Earth-orbiting telescopes composed of small modules deployed in a phased manner to outer Solar System exploration missions able to adapt to new mission roles and changing science targets. Human spaceflight activities will also benefit from failure-robust reconfiguration techniques that enable expansions to space stations or self-repair and adaptation of manned vehicles beyond low Earth orbit.

This paper described a potential low-power, robust method to reconfigure modular space systems by stating the problem of reconfiguration from one shape to another as a stepwise sequence of kinematics and passively stable dynamics rather than as an active tracking problem. A spacecraft system undergoing such a reconfiguration maneuver achieves low control and computation effort by taking advantage of the ambient force fields naturally present in the space environment, such as gravity, or augmenting these forces with additional force fields from passive sources, such as permanent magnets. The passive dynamics of the system add robustness by reducing the number of actuators required for reconfiguration and placing the onus of regulating the maneuver on multibody kinematics rather than an on-board control system. This strategy gives the system determinacy in each step of the reconfiguration, in the sense that the system moves towards known dynamic equilibria. Operators can confirm the system configuration at each of these "safe steps." Should any problem arise during the process, the spacecraft will naturally fall into a stable equilibrium configuration, from which recovery operations can safely take place.

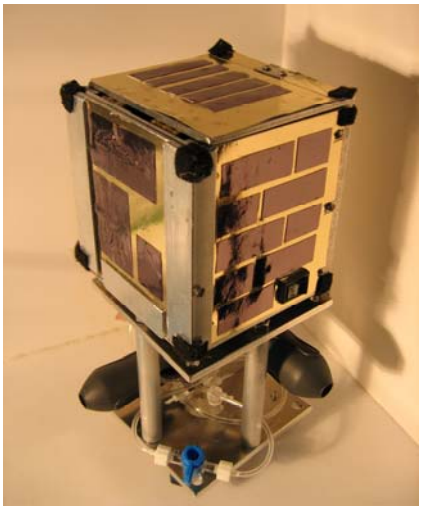

Figure 8. Air-levitated, CubeSat-sized laboratory demonstration unit.

In addition, this work developed a simulation environment for multibody spacecraft simulations, based on the equation of motion formulation advocated by Udwadia and Kalaba. Those equations of motion have been adapted to account for full three-dimensional rigid body dynamics with quaternion states. The MATLAB simulation environment is object-oriented, extensible, and allows access to the full system state for analysis during and after simulation. Simulations of

example multibody spacecraft architectures provide a means to explore the full tree of possible sequential-equilibrium reconfigurations for a given system, thus determining the reachable configurations and control input sequence of kinematics to reach them. These simulation tools have numerous other applications to multibody dynamics problems, as well.

In the future, laboratory testbeds will demonstrate implementations of these reconfiguration algorithms and control strategies. The enumeration approach for constructing reconfiguration graphs outlined in Section IV is generalizable to many multibody space systems. Air-levitated spacecraft simulator systems in the laboratory, such as the one shown in Figure 9, and future NASA microgravity flights will verify that the enumeration algorithm identifies the possible equilibrium configurations and the proper connectivity between them. With a reconfiguration graph in hand, these systems will also demonstrate practical implementations of reconfiguration control through sequential equilibria and provide data on power usage and fault tolerance of the control strategy to sensing, actuation, or control failures in a real system.

These theoretical tools have applications to more general reconfigurable systems than those linked by magnetic flux pinning or other non-contacting forces. They apply to any systems which can alter kinematic constraints, modify connectivity between bodies, or apply force fields. The logical extension from applied force fields to body forces and torques will generalize these methods to many other reconfiguration problems, as well, though in such cases the system will not have the stability guarantees of stable potential wells. The techniques and data from this research may enable new classes of reconfigurable space systems or enhance the capabilities of existing and next-generation space systems.

References

[1] Dong, S. et al. "Self-assembling wireless autonomously reconfigurable module design concept," *Acta Astronautica*, Vol. 62, 2008, pp.246-256.

[2] McCamish, S.B., Romano, M., Nolet, S., Edwards, C.M., and Miller, D.W. "Ground and Space Testing of Multiple Spacecraft Control During Close-Proximity Operations." *AIAA Guidance, Navigation, and Control Conference*, paper 2008-6664. AIAA, Honolulu, HI, 2008.

[3] Rui, C., Kolmanovsky, I., and McClamroch, N. H. "Nonlinear Attitude and Shape Control of Spacecraft with Articulated Appendages and Reaction Wheels." *IEEE Transactions on Automatic Control*, Vol. 45, No. 8, 2000, pp.1455-1469.

[4] Rehnmark, F., Pryor, M., Holmes, B., Pedreiro, N., and Carrington, C.. "Development of a Deployable Nonmetallic Boom for Reconfigurable Systems of Small Modular Spacecraft," *48th AIAA/ASME/ASCE/AHS/ASC Structures, Structural Dynamics, and Materials Conference*, AIAA, Honolulu, HI, 2007.

[5] Xia, C., Wang, P., and Hadaegh, F., "Optimal Formation Reconfiguration of Multiple Spacecraft with Docking and Undocking Capability," *Journal of Guidance, Control, and Dynamics*, Vol. 30, No. 3, 2007, pp. 694-702.

[6] LeMaster, E., Schaechter, D., and Carrington, C., "Experimental Demonstration of Technologies for Autonomous On-Orbit Robotic Assembly," *Space 2006 Conference*, AIAA, San Jose, CA, 2006.

[7] Shoer, J. and Peck, M. "Sequences of Passively Stable Dynamic Equilibria for Hybrid Control of Reconfigurable Spacecraft." *AIAA Guidance, Navigation, and Control Conference*, paper 2009-5800, AIAA, Chicago, IL, 2009.

[8] Schaub, H., Parker, G. G. and King, L. B. "Challenges and Prospects of Coulomb Spacecraft Formations," *Journal of the Astronautical Sciences*, Vol. 52, Nos. 1–2, 2004, pp. 169–193.

[9] Kong, E.M.C, Kwon, D.W., Schweighart, S.A., Elias, L.M., Sedwick, R.J. and Miller, D.W. "Electromagnetic Formation Flight for Multi-Satellite Arrays." *Journal of Spacecraft and Rockets*, Vol 41, No. 4, 2004, pp. 659-666.

[10] Shoer, J., and Peck, M. "Flux-Pinned Interfaces for the Assembly, Manipulation, and Reconfiguration of Modular Space Systems." *Journal of the Astronautical Sciences*, 2010 (*to appear*).

[11] Shoer, J. and Peck, M. "Stiffness of a Flux-Pinned Virtual Structure for Modular Spacecraft." *Journal of the British Interplanetary Society*, vol. 62, no. 2, pp. 57-65, 2009.

[12] Shoer, J. and Peck, M. "Reconfigurable Spacecraft as Kinematic Mechanisms Based on Flux-Pinning Interactions." *Journal of Spacecraft and Rockets*, vol. 46, no. 2, pp. 466-469, 2009.

[13] Norman, M. "Stationkeeping of a flux-pinned satellite network." *AIAA Guidance, Navigation and Control Conference and Exhibit*, paper 2008-6475. Honolulu, HI, 2008.

[14] Jones, L. "Prospects and Challenges of Particulate Solar Sail Propulsion." *AIAA/AAS Astrodynamics Specialist Conference and Exhibit*, paper 2008-7077. Honolulu, HI, 2008.

[15] Gersh, J. "Architecting the Very-Large-Aperture Flux-Pinned Space Telescope: A Scalable, Modular Optical Array with High Agility and Passively Stable Orbital Dynamics." *AIAA/AAS Astrodynamics Specialist Conference and Exhibit*, paper 2008-7212. AIAA/AAS, Honolulu, HI, 2008.

[16] Brandt, E. H., "Rigid levitation and suspension of high-temperature superconductors by magnets," *American Journal of Physics*, Vol. 58, No. 1, 1990, pp. 43-49.

[17] Davis, L. C., "Lateral restoring force on a magnet levitated above a superconductor," *Journal of Applied Physics*, Vol. 67, No. 5, 1990, pp. 2631-2636.
[18] Schonhuber, P. and Moon, P. C., "Levitation forces, stiffness, and force-creep in YBCO high-T_c superconducting thin films," *Applied Superconductivity*, Vol. 2, No. 7, 1994, pp. 523-534.
[19] Shoer, J., Wilson, W., Jones, L., Knobel, M., and Peck, M. "Microgravity Demonstration of Flux Pinning fot Station-Keeping and Reconfiguration of CubeSat-Sized Spacecraft." *Journal of Spacecraft and Rockets*, 2010 (*submitted*).
[20] Wilson, W., Shoer, J., and Peck, M. "Demonstration of a Magnetic Locking Flux-Pinnged Revolute Joint for Use on CubeSat-Standard Spacecraft." *AIAA Guidance, Navigation and Control Conference and Exhibit*, paper AIAA-2009-5904. AIAA, Chicago, IL, 2009.
[21] Udwadia, F. and Kalaba, R. *Analytical Dynamics: A New Approach*. Cambridge University Press, 2007.
[22] Toumela, J. "Kinematic Analysis of Multibody Systems." *BIT Numerical Mathematics*, Vol. 48, No. 2, 2008, pp. 405-412.
[23] Gu, E.Y.L. "Configuration Manifolds and Their Applications to Robot Dynamic Modeling and Control." IEEE Transactions of Robotics and Automation, Vol. 16, No. 5, 2000, pp.517-527.
[24] Henzinger, T.A. "The Theory of Hybrid Automata." *Proceedings of the 11th Annual Symposium on Logic in Computer Science (LICS)*, IEEE Computer Society Press, 1996, pp. 278-292.
[25] Kordyuk, A. "Magnetic levitation for hard superconductors," *Journal of Applied Physics*, Vol. 83, No. 1, 1998, pp. 610-612.
[26] Udwadia, F. and Phohomsiri, P. "Explicit equations of motion for constrained mechanical systems with singular mass matrices and applications to multi-body dynamics." *Proceedings of the Royal Society A*, Vol. 462, 2006, pp. 2097-2117.

On page 7, the equation describing the transformation matrix T should read:

$$\begin{aligned} {}^{B}\omega^{B/N} &= 2[(-q_{123}^{\times} + q_4 1_3) \quad -q_{123}]\dot{q} \\ {}^{B}\omega^{B/N} &= T(q)\dot{q} \end{aligned} \tag{7}$$

On page 8, the equation defining the spherical joint constraint matrix should be:

$$\begin{aligned} A_{r_B} &= 1_3 \\ A_{N_{q^B}} &= -\left({}^{N}Q^{B}\,{}^{B}p_{BC}\right)^{\times}\,{}^{N}Q^{B}T_B \\ A_{r_C} &= -1_3 \\ A_{N_{q^C}} &= \left({}^{N}Q^{C}\,{}^{C}p_{CB}\right)^{\times}\,{}^{N}Q^{C}T_C \\ b &= \left(\left({}^{N}Q^{C}T_C\dot{q}_C\right)^{\times}\right)^{2}\,{}^{N}Q^{C}\,{}^{C}p_{CB} + \left({}^{N}Q^{C}\,{}^{C}p_{CB}\right)^{\times}\,{}^{N}Q^{C}\dot{T}_C\dot{q}_C - \left(\left({}^{N}Q^{B}T_B\dot{q}_B\right)^{\times}\right)^{2}\,{}^{N}Q^{B}\,{}^{B}p_{BC} \\ &\quad - \left({}^{N}Q^{B}\,{}^{B}p_{BC}\right)^{\times}\,{}^{N}Q^{B}\dot{T}_B\dot{q}_B. \end{aligned} \tag{18}$$

One expression for the constraint matrices for a revolute joint or hinge with its rotation axis aligned with a unit vector $\hat{\boldsymbol{a}}$ that is fixed on the body B is a combination of two spherical joints displaced along the rotation axis from one another:

$$\begin{aligned} A_{r_B} &= \begin{bmatrix} 1_3 \\ 1_3 \end{bmatrix} \\ A_{N_{q^B}} &= \begin{bmatrix} -\left({}^{N}Q^{B}\left({}^{B}p_{BC} + {}^{B}\hat{a}\right)\right)^{\times}\,{}^{N}Q^{B}T_B \\ -\left({}^{N}Q^{B}\left({}^{B}p_{BC} - {}^{B}\hat{a}\right)\right)^{\times}\,{}^{N}Q^{B}T_B \end{bmatrix} \\ A_{r_C} &= -\begin{bmatrix} 1_3 \\ 1_3 \end{bmatrix} \\ A_{N_{q^C}} &= \begin{bmatrix} \left({}^{N}Q^{C}\left({}^{C}p_{CB} + {}^{C}Q^{B}\,{}^{B}\hat{a}\right)\right)^{\times}\,{}^{N}Q^{C}T_C \\ \left({}^{N}Q^{C}\left({}^{C}p_{CB} - {}^{C}Q^{B}\,{}^{B}\hat{a}\right)\right)^{\times}\,{}^{N}Q^{C}T_C \end{bmatrix} \\ b &= \begin{bmatrix} \left(\left({}^{N}Q^{C}T_C\dot{q}_C\right)^{\times}\right)^{2}\,{}^{N}Q^{C}\left({}^{C}p_{CB} + {}^{C}Q^{B}\,{}^{B}\hat{a}\right) + \left({}^{N}Q^{C}\left({}^{C}p_{CB} + {}^{C}Q^{B}\,{}^{B}\hat{a}\right)\right)^{\times}\,{}^{N}Q^{C}\dot{T}_C\dot{q}_C - \left(\left({}^{N}Q^{B}T_B\dot{q}_B\right)^{\times}\right)^{2}\,{}^{N}Q^{B}\left({}^{B}p_{BC} + {}^{B}\hat{a}\right) - \left({}^{N}Q^{B}\left({}^{B}p_{BC} + {}^{B}\hat{a}\right)\right)^{\times}\,{}^{N}Q^{B}\dot{T}_B\dot{q}_B \\ \left(\left({}^{N}Q^{C}T_C\dot{q}_C\right)^{\times}\right)^{2}\,{}^{N}Q^{C}\left({}^{C}p_{CB} - {}^{C}Q^{B}\,{}^{B}\hat{a}\right) + \left({}^{N}Q^{C}\left({}^{C}p_{CB} - {}^{C}Q^{B}\,{}^{B}\hat{a}\right)\right)^{\times}\,{}^{N}Q^{C}\dot{T}_C\dot{q}_C - \left(\left({}^{N}Q^{B}T_B\dot{q}_B\right)^{\times}\right)^{2}\,{}^{N}Q^{B}\left({}^{B}p_{BC} - {}^{B}\hat{a}\right) - \left({}^{N}Q^{B}\left({}^{B}p_{BC} - {}^{B}\hat{a}\right)\right)^{\times}\,{}^{N}Q^{B}\dot{T}_B\dot{q}_B \end{bmatrix}. \end{aligned} \tag{19}$$

These are the equations implemented in the current (1.3) version of QuIRK.